ADVANCED OPTICAL MATERIALS
www.advopticalmat.de

Highly Efficient Photoluminescence and Lasing from Hydroxide Coated Fully Inorganic Perovskite Micro/Nano-Rods

Guanhua Ying, Atanu Jana, Vitaly Osokin, Tristan Farrow, Robert A. Taylor, and Youngsin Park**

The effect of surface passivation on the photoluminescence (PL) emitted by $CsPbBr_3$ micro/nano-rods coated with $Pb(OH)_2$ is investigated, where a high quantum yield and excellent stability for the emission are found. The $CsPbBr_3$/$Pb(OH)_2$ rods generally present a peak that is blue shifted compared to that seen in rods without a hydroxide cladding at low temperatures. By increasing the temperature, it is further shown that the passivated surface states are very robust against thermal effects and that the PL peak intensity only drops by a factor of 1.5. Localized stimulated emission at defect states found within larger rods is also demonstrated, clarified by spatially resolved confocal PL mapping along the length of the rods. The diffusion parameter of the carrier density distribution is measured to be 5.70 µm for the sky-blue emission, whereas for the defect lasing site it is found to be smaller than this excitation spot size.

1. Introduction

All-inorganic lead halide perovskite materials have produced a huge impact on optoelectronic applications including solar cells, light emitting diodes, and lasing devices in the past few years.[1–10] One big advantage over their organic counterparts is their high stability leading to tolerance toward chemical environment, temperature, and light exposure.[11,12] Despite this, a remaining key vulnerability is from water due to the highly ionic structure of perovskites,[13] which can cause problems in realistic devices. Passivation methods using zwitterions,[14] organic–inorganic hybrid ion pairs[15] and metal oxides[16–18] show promise in water-related stabilization. Even water itself can be used in some synthesis techniques.[19–22] While the room temperature characteristics have been well studied, investigations at cryogenic temperatures are essential to gain a proper understanding of the physics underpinning the origin of any induced qualitative improvements. Studies into inorganic perovskite nanocrystals[23,24] as well as nanowires[25] at low temperatures indeed lead to interesting optical phenomena and interpretations of carrier-level physics.

Here, we present the direct observation of interface states and defect lasing sites from $Pb(OH)_2$ coated $CsPbBr_3$ micro/nano-rods with different diameters. The fully inorganic rods with hydroxide cladding are prepared as described in detail in a previous growth paper.[26] A temperature dependent study shows that the passivated surface states are very robust against thermal effects and the photoluminescence (PL) peak intensity only drops by a factor of 1.5 from 4 K to room temperature. A comparison of the interface emission to uncoated $CsPbBr_3$ also provides a link between the modified spectrum and the original $CsPbBr_3$ emission. Localized defect emission sites are seen within thicker rods at low temperature, which are shown to exhibit bright stimulated emission through an electron–hole plasma. We also present a direct observation of diffusion from both interface and defect sites using a confocal micro-PL (µPL) mapping system with separable excitation and collection regions to further support our conclusions.

2. Results and Discussion

The crystal structure was characterized by powder X-ray diffraction and the sample was found to exhibit the cubic phase (Figure S1, Supporting Information). Transmission electron microscopy images are shown in **Figure 1**, where the interface between the perovskite and hydroxide layer can be seen clearly in Figure 1c. For µPL measurements, the solution $CsPbBr_3$ rods were dispersed on an Au pattern SiO_2 substrate as shown in

G. Ying, V. Osokin, Dr. T. Farrow, Prof. R. A. Taylor
Clarendon Laboratory
Department of Physics
University of Oxford
Parks Road, Oxford OX1 3PU, UK
E-mail: robert.taylor@physics.ox.ac.uk
Dr. A. Jana
Division of Physics and Semiconductor
Dongguk University
Seoul 04620, Korea
Dr. T. Farrow
Centre for Quantum Technologies
National University of Singapore
Science Drive 2, Singapore 117543, Singapore
Prof. Y. Park
School of Natural Science
Ulsan National Institute of Science and Technology (UNIST)
Ulsan 44919, Korea
E-mail: ysinpark@unist.ac.kr
The ORCID identification number(s) for the author(s) of this article can be found under https://doi.org/10.1002/adom.202001235.

DOI: 10.1002/adom.202001235

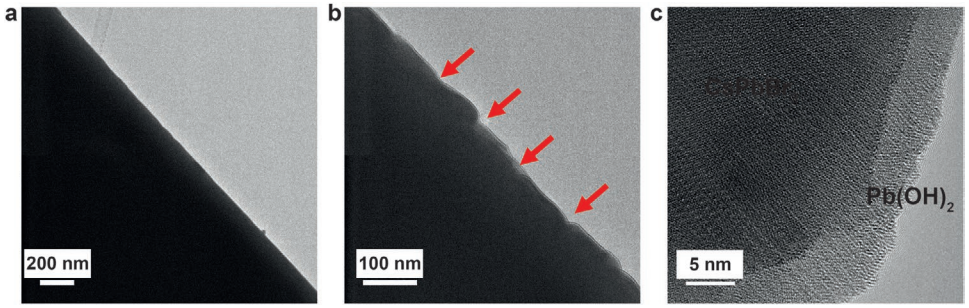

Figure 1. a) Transmission electron microscopy images of the $CsPbBr_3$ rods coated with $Pb(OH)_2$. The red arrows in (b) indicate the surface defect regions. c) The high-resolution image at a corner. The interface between $CsPbBr_3$ and $Pb(OH)_2$ is not critical and defects were observed in $Pb(OH)_2$.

a scanning electron microscopy image (Figure S2, Supporting Information). The thickness of the $Pb(OH)_2$ on the periphery of different nanorods varies by a few nanometres. Once the 5–10 nm thick $Pb(OH)_2$ layer has formed on top of the nanorods, OH^- ions can no longer penetrate into the structure and thus the thickness of the $Pb(OH)_2$ layer around different nanorods is quite consistent.

Figure 2 shows the excitation power-dependent μPL spectra of $Pb(OH)_2$ coated $CsPbBr_3$ rods with different diameters of 1 (rod-A), 2.5 (rod-B), and 4 μm (rod-C). Schematic diagrams and optical microscopy (OM) images are presented in the upper panels. A 450 nm pulsed laser beam of area 1 μm^2 was focused onto the middle of the samples. The OM image clearly shows guided emission emerging from the ends of the rods, which is in good agreement with previously reported results.[10,11,27,28] For the rod-A, a broad emission near 495 nm (sky-blue) was observed (Figure 2a). This peak is blue shifted compared to the normal emission from $CsPbBr_3$ systems such as quantum dots, nanocrystals, nanowires, and films of 520–540 nm.[10,12,14,27–37] In these studies, the signature $CsPbBr_3$

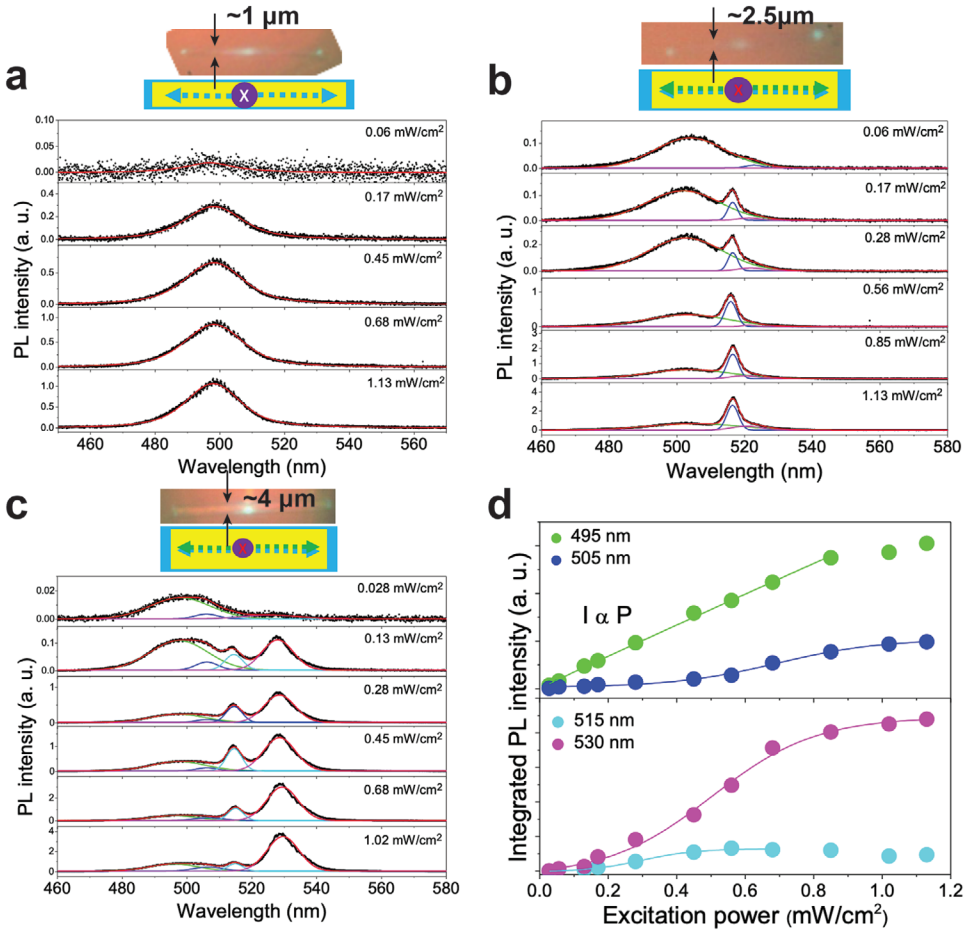

Figure 2. Power-dependent μPL spectra measured at $CsPbBr_3$ rods with three different diameters: a) ≈1 μm, b) ≈2.5 μm, and c) ≈4 μm. All the emission peaks were fitted. The black dot circles are the data and the solid colored lines are fits and reconstructed peaks. d) Integrated PL intensity of the sample C as a function of excitation power.

emission sits in consistent wavelength regions and its intensity increases linearly with excitation power, indicating an excitonic origin. As for rod-B, an additional emission peak protrudes at ≈518 nm (Figure 2b). Its intensity increases rapidly with excitation power following a S-shaped dependence, which is consistent with similar lasing seen by other researchers attributed to biexcitonic emission.[27,28,31,32]

In the case of bigger rods of width ≈4 µm, an excitation power run shows the emergence of a new green emission peak near 530 nm (Figure 2c) at relatively high pumping power. In order to extract detailed intensity variation, all the spectra were fitted using Gaussian profiles with the integrated intensity taken as a function of excitation power as presented in Figure 2d. Apart from the two emissions described above, new emission sites are observed at wavelengths of 505 and 530 nm. As we expected, the excitonic peak increases linearly with excitation power, whereas the others show an S-shape behavior and hence originate from stimulated emission where the cavity can be formed by both the lateral and vertical sides of the rod (Figure S3, Supporting Information) or due to the localization of carriers where population inversion results in preferential emission.

Such a shift of 30 nm for the sky-blue emission from the well-studied $CsPbBr_3$ PL peak at around 535–540 nm is caused by the presence of the $Pb(OH)_2$ cladding on the perovskite surface via a reaction with the OH^- ions. Labile peripheral $[PbX_6]^{4-}$ octahedrals are replaced by a $Pb(OH)_2$ bonded interface to strengthen the surface stability and introduce surface passivation. Proof of successful bonding can be seen in our earlier paper.[26] Moreover, such an emission shift can't be due to residual MA^+ cations not only because it is experimentally verified that no MA^+ signal is seen in Fourier Transform Infrared Spectroscopy[26] but also from the fact that hybridizing with a larger cation in the unit cell will lead to a spectral shift in a direction opposite to that observed. In addition, the transition in $Pb(OH)_2$ itself is also too far from this wavelength range. With this surface cladding, the cubic structure of $CsPbBr_3$ is altered into a rod like structure and the actual thickness of the perovskite layer is thinner than that measured from the outermost dimension. To examine the remaining octahedrals relating to the original $CsPbBr_3$ structure EDX images are shown together with an SEM image taken from the same region (Figure S4, Supporting Information).

Temperature dependent µPL studies for rod-A and rod-C are shown (**Figure 3**). At 4.5 K, PL spectra of both rods exhibit emission peaks within a wavelength range of 495–510 nm. The relatively uniform distribution verifies that the central perovskite core is still preserved. While the sky-blue emission site is seen in all of our rods at all temperatures, green peaks at 540 nm matching the $CsPbBr_3$ signature wavelength are seen locally in thicker rods. The details of these emissions will be discussed later.

As the temperature increases toward 298 K, we noticed that while the green $CsPbBr_3$ emission in rod-C blue shifts in agreement with the typical trend observed in perovskite materials, the sky-blue emission red shifts in both cases (Figure 3a,b). Figure 3b shows that this red-shift leads to a merging with the peak arising from the uncoated perovskite green emission and eventually reproduces the $CsPbBr_3$ room temperature spectrum peaking between 515 and 520 nm.[38,39] The sky-blue emission taken below 150 K for both rods has an asymmetric and almost unbroadened energy distribution with more tail states associated with the higher energy side. It is then clear that the energy transition of the radiative process at the cladding

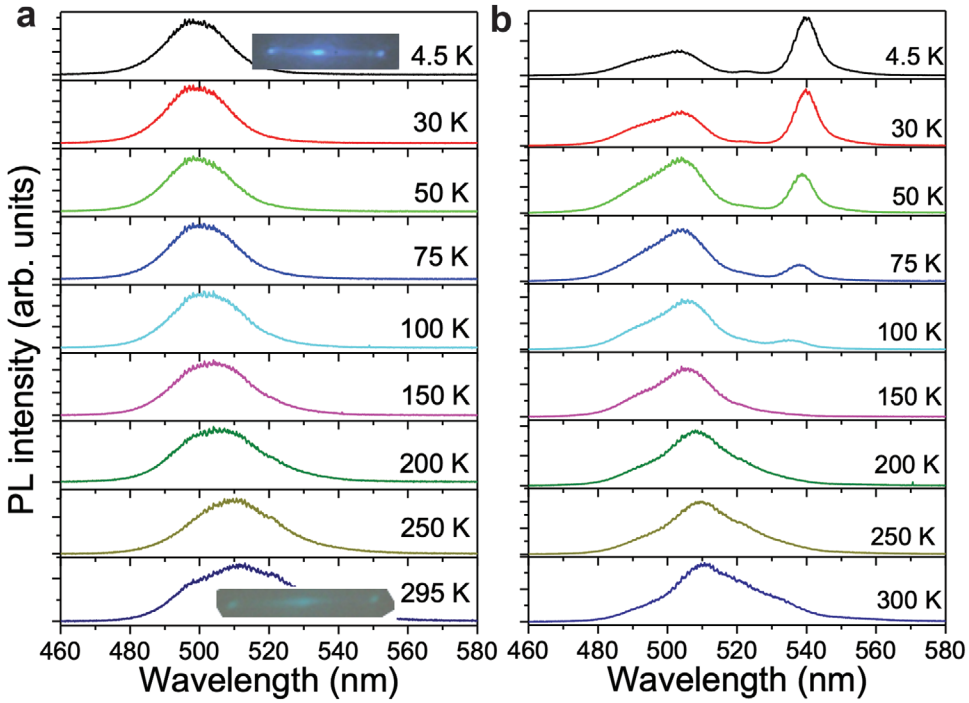

Figure 3. Temperature-dependent PL spectra of the rods with diameters of a) ≈1 µm and b) ≈4 µm. The insets in (a) depict the actual PL optical microscopy images taken at low and room temperature. The sky-blue emission is clearly seen at 4.5 K and the green emission is seen at room temperature.

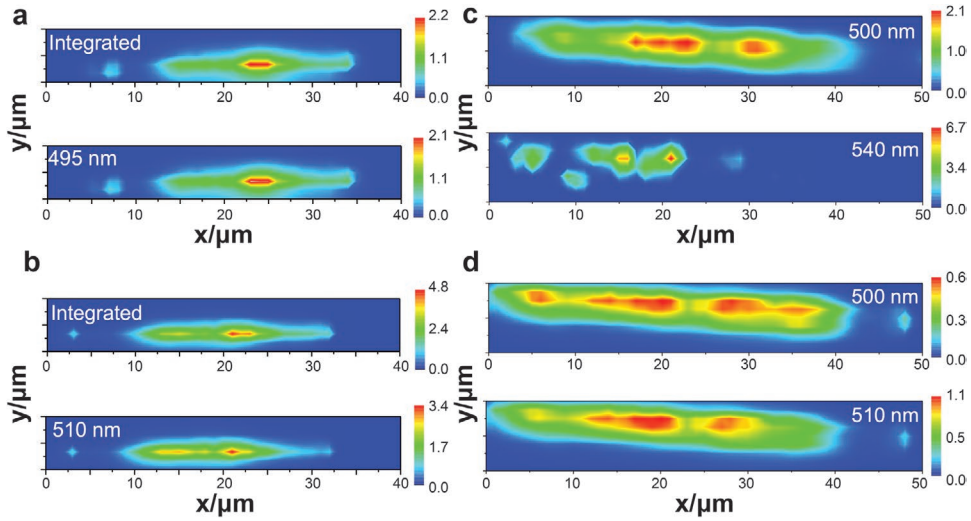

Figure 4. Spatial PL maps of rods with diameters of a,b) ≈1 μm and c,d) ≈4 μm. a) Map of integrated and single emission wavelength of the 495 nm measured at 4.5 K. b) Map of integrated and single emission wavelength of 510 nm measured at 295 K. c) Map of the single emission wavelengths of 500 and 540 nm measured at 4.5 K. d) Mapping of the single emission wavelengths of 500 and 510 nm measured at 295 K.

interface splits from that of unpassivated $CsPbBr_3$ as the temperature goes down. In the case of thinner rods (Figure 3a), almost all the exciton recombination occurs at the interface. Another noteworthy feature is that the PL intensity from the sky-blue emission only decays by a factor of ≈1.5 from 4.5 K to room temperature (Figure S5, Supporting Information), while that in all other reported perovskite cases undergoes a reduction of 100 or more to the best of our knowledge. Therefore, the interface states are less vulnerable to thermal effects and this can explain why the cladding helps improving the internal quantum efficiency.

Spatially resolved confocal μPL maps of rod-A and rod-C filtered at the main wavelengths of interest are shown for 4.5 and 298 K in **Figure 4**. A comparison with rod-A at both temperatures can be seen (Figure 4a,b). At room temperature, both rods show relatively uniform intensity distributions all originating from the interface emission in agreement with the merged single spectrum toward high temperature. However, much more localized green emission at 540 nm is seen for rod-C at 4.5 K (Figure 4c). In contrast, the PL intensity distribution for the 495 nm sky-blue emission from both rods is the same as that at room temperature. This is because the $Pb(OH)_2$ cladding is formed uniformly around the surface of those rods and confirms that this emission originates from the perovskite–cladding interface. The reason why there are no local green emission sites in the thinner rod is that the core perovskite cross section is on a scale of hundreds of nanometers and hence the lattice strain is distributed smoothly between it and the $Pb(OH)_2$ interfaces. In the case of the thicker rod, due to the larger size of the core region there can be significant lattice mismatch between the interface and inner uncoated perovskite. The resulting built-in strain can cause a discontinuity of the lattice and hence introduce defect sites. Such defect sites can act as traps and lead to localization of excitons.

In order to investigate the emission in rod-C, we used a μPL system capable of exciting and collecting luminescence from different positions on the sample as illustrated in **Figure 5**a. A piezo-electric mirror is used to scan the excitation laser beam within the small angle approximation of the objective, where linearity is maintained. A small tilt to the beam path introduces a translational movement of the focused laser spot while the objective itself is not influenced. The setup is hence capable of decoupling the excitation and collection when this linear approximation is preserved. Such added degree of freedom enables various new scanning modes including either fixing excitation or collection and scanning the other. The scan can give spatial resolution area of 1 μm^2, and here we used it to study the excitation power dependence. The PL spectra measured with excitation and detection both situated at one end is shown (Figure 5b). The two emissions observed near at 522 and 538 nm are again seen to arise from stimulated emission. However, these emission wavelengths are slightly different to the emission (515 and 529 nm) measured at center-excitation and detection (Figure 2c). Almost no sky-blue emission at ≈495 nm is seen due to the fact that the morphology at the end of the rods is less regular and $Pb(OH)_2$ coverage is bad, which can be used again as evidence for verifying the identity of the sky-blue emission as from interface passivated emission. In addition, this further proves that the green stimulated emission is decoupled from the sky-blue emission. The nature of the green stimulated emission is likely to be associated with the creation of an electron–hole plasma. The initial formation of hot electron–hole plasma presents a broad energy distribution before cooling down to the individual cavity modes and is hence consistent with the relatively wide stimulated emission line observed in our spectra. This green emission is linked to the signature emission wavelength of $CsPbBr_3$ at around 520 nm and hence a slight red shift in emission wavelength can result from the coupling to plasmon resonance which relaxes the energy requirement for population inversion. Such a red-shift can also occur in bi-excitonic lasing, however, in this case the line width tends to be narrower and the red-shift in emission energy is expected to be large. Given our relatively high-power pulsed excitation, it is also certain that the lasing we observed is not linked to exciton-polaritons. Another power run was performed by keeping the collection at the end of the rod and the excitation

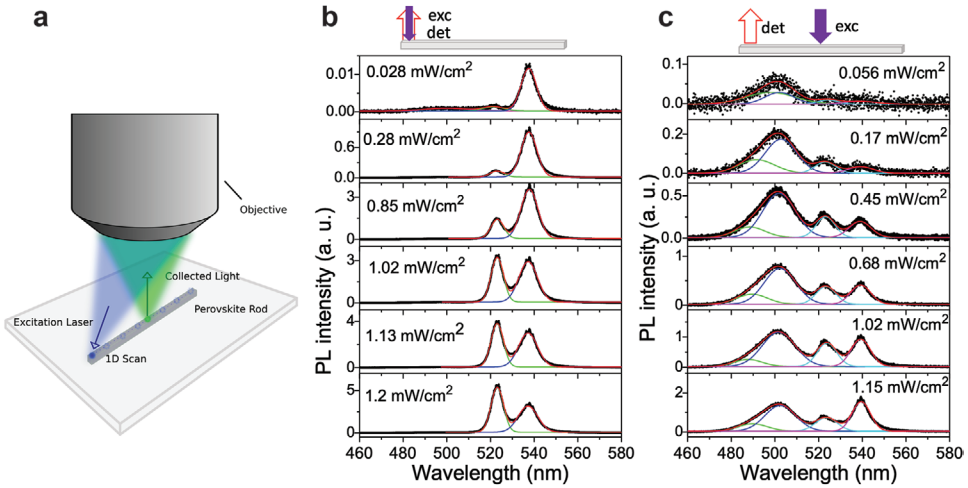

Figure 5. Power-dependent separable excitation-collection μPL spectra measured at $CsPbBr_3$ rods with a diameter of ≈4 μm. a) Schematic of separable excitation and collection μPL operation, the blue excitation laser spot is controlled via a scanning mirror independently to the objective-controlled collection site within the small angle approximation of the lens. b) The excitation and detection positions are the same at the end site of the rod. c) The excitation and detection positions are separated at the center site and one end site of the rod. All emission peaks were fitted. The black dot circles are the measured data and the solid color lines are fitted and reconstructed peaks.

at the center (Figure 5c). The resulting spectra once more demonstrate that the sky-blue emission from the interface is again observable. This hints that exciton transport within the interface layer can be very long. No emission at either 515 or 530 nm is seen (Figure 5c). This confirms that stimulated emission at defect sites is limited to the confined regions only. All the peaks are slightly red-shifted and this is predicted as the photons with higher energy undergo stronger re-absorption when propagating along the rod.

The spatial profile of excitons at 4.5 K is further investigated measured at excitation power of 0.28 μW cm^{-2} by fixing the excitation at the center and scanning the collection along the rod (**Figure 6**a). Study of carrier density distribution was performed via spatially resolved time-integrated PL to extract information relating to diffusion. A Gaussian profile is fitted and the diffusion parameters are extracted and found to be ≈5.70 and ≈1.12 μm, respectively. This number is of direct correspondence to the ability of carriers to travel inside a solid matter. It is clear then that lasing emission at the green site is indeed much localized with little diffusion apparent before recombination. Moreover, localization is expected to happen at even smaller region as the spatial resolution is limited by our focused laser spot size of ≈1 μm. On the other hand, the blue emission exhibits a very long diffusion length. As the diffusion length of the $CsPbBr_3$ nanocrystals were widely reported from 290 nm to 9.2 μm,[40,41] our values are quite valid. A time resolved PL (TRPL) comparison of the two peaks is shown (Figure 6b). The green lasing lifetime is significantly shorter than that of the sky-blue decay and is calculated to have a lifetime of 182 ps after convoluting the signal with our instrument response function (IRF). This is expected since it arises from stimulated emission (Figure 6c). Since localization increases carrier density at the defect site, stimulated emission is hence enhanced due to the large population of localized carriers present. An electron–hole plasma is created locally near the excitation laser spot. The associated fast decay then limits carriers from escaping and results in a very short diffusion length but a bright emission intensity. On the other hand, surface passivation through $Pb(OH)_2$ stabilizes the peripheral structure and reduces the density of edge states. Therefore, diffusion of the excitons through the interface is enhanced.

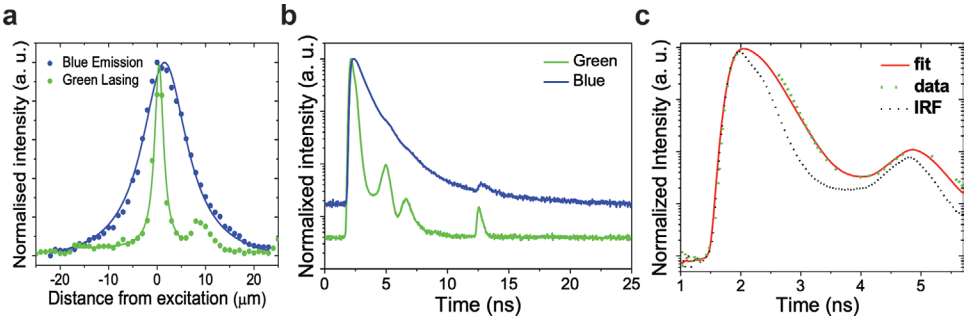

Figure 6. a) 1D μPL collected emission scan with fixed excitation at the center for the sky-blue interface site and green defect site. Both are fitted by Gaussian profile to extract diffusion lengths of 5.70 and 1.12 μm, respectively. b) Time-resolved comparison of the interface and defect emissions. The defect emission has a decay lifetime in the picosecond regime limited by the instrument response function. The multiple peaks arise form electronic reflections in the TCPC system. c) Time-resolved photoluminescence of the green emission with IRF.

3. Conclusion

In summary, we have characterized enhanced PL due to surface passivation from a $Pb(OH)_2$ coating of $CsPbBr_3$ rods of various diameters via time-integrated and time-resolved μPL analysis. The PL peak of the $CsPbBr_3/Pb(OH)_2$ rod shows excitonic emission at a sky-blue wavelength near 495 nm, which is blue-shifted compared to that of uncoated $CsPbBr_3$ structure. Narrower lines falling within the wavelength range of 520–540 nm are observed only in rods with a larger diameter (≈4 μm) and arise from stimulated emission. Spatially resolved confocal PL mapping was performed along the rod and shows that the stimulated emission is only confined locally within an area limited by our confocal resolution. Temperature-dependent PL intensity variation of the sky-blue emission indicates a drop of only 1.5 from 4 K to room temperature implying high PL quantum efficiency. An accompanying red-shift due to confinement is also observed with increasing temperature. By adding the functionality of fully separable excitation and collection scanning to our confocal microscopy, we measured the diffusion parameters of the sky-blue and green emissions to be ≈5.70 μm and ≤1.1 μm, respectively, indicating not only that the exciton transport within the interface layer can be very long but also that the stimulated emission is confined to defect spots. The decay times are further extracted to be 865 and 182 ps for the excitonic transition of the sky-blue site and stimulated emission of the green site, being consistent with the nature of the two emissions.

4. Experimental Section

Materials and Synthesis of $CsPbBr_3$ Rods: In a typical synthesis, first Cs_2CO_3 (500 mg, 1.5 mmol) was added to a 2 mL HBr solution of $PbBr_2$ (1 g, 2.7 mmol) in a small bottle and the bright yellow precipitate of bulk $CsPbBr_3$ appeared immediately as an intermediate product. It was then left in closed bottle filled with methylamine solution for one day until its appearance turned greenish white where $Pb(OH)_2$ was formed at the surface of $CsPbBr_3$. The methylamine reacted with water generating hydroxide ions in solution. These hydroxide ions reacted with the $CsPbBr_3$ and formed $Pb(OH)_2$-coated $CsPbBr_3$. The final water-stable $CsPbBr_3$ structure was obtained after ten days. The product was washed several times with plenty of water and dried under vacuum at 60 °C. The diameter of the $Pb(OH)_2$-coated $CsPbBr_3$ rods could be tuned by varying the reaction time (days). As the methylamine gas slowly diffused into the solution, the atmospheric temperature was also a crucial factor for the evaporation of methylamine gas, which created OH^- ions by reacting with water. More homogeneous samples could be prepared by keeping the rods for one month in closed conditions. During the sample preparation, the atmospheric temperature was maintained at 20 °C.

Structural Characterization: The powder X-ray diffraction was done on a D/MAX2500V/PC diffractometer, Rigaku using a Cu-rotating anode X-ray system (Figure S1, Supporting Information). The Bragg diffraction angle (2θ) range was set to 10–50° and the scan rate was 2° min^{-1}. Transmission electron microscopy images were taken on a JEOL JEM-2100F electron microscope using a 200 kV electron source. Samples were prepared on 200-mesh carbon coated Cu grids by dropping nanocrystal solutions, which were then allowed to evaporate.

Optical Characterization: In order to measure the μPL, the solution of $CsPbBr_3$ rods was dispersed on an Au patterned SiO_2 substrate to determine the position of clusters with different sizes. The scanning electron microscopy image is shown in Figure S2, Supporting Information. A pulsed 450 nm laser operating at 40 MHz was used as an excitation source through a confocal setup. The sample was mounted in a continuous-flow helium cryostat, allowing the temperature to be controlled accurately from 4.5 K to room temperature. A 100 × long working distance apochromatic objective was held by a sub-micron precision piezoelectric stage above the cryostat and used to focus the incident laser beam to a spot size of ≈1 μm^2 and to collect the resulting luminescence. The luminescence was then directed to a 0.3 m focal length spectrometer with a 1200 g mm^{-1} grating giving a spectral resolution of ≈700 μeV. The signal was finally detected using a cooled charge coupled device detector. A telecentric lens arrangement was also present allowing the incident angle of the exciting laser at the entrance to the objective to be varied by a computer-controlled mirror thus provided an independent means to move the exiting spot relative to the collected emission, which was imaged confocally through the center of the objective. TRPL measurements were carried out using the same experimental set up as above. The dispersed PL was reflected toward a photomultiplier connected to a commercial photon counting system (Picoquant Time Harp). Measurements of the lifetimes of the confined states were then carried out over a range of excitation power densities.

Supporting Information

Supporting Information is available from the Wiley Online Library or from the author.

Acknowledgements

This work was supported from the Basic Science Research Program through the National Research Foundation of Korea (NRF) (2018R1D1A1B07043676) and also by grant DKR00940 on Quantum Materials from Shanghai Tech University, China.

Conflict of Interest

The authors declare no conflict of interest.

Keywords

$CsPbBr_3$ rods, long diffusion length, $Pb(OH)_2$ coating, perovskite/hydroxide interface, sky-blue emission, spatially resolved confocal mapping, surface passivation

Received: July 21, 2020
Revised: September 3, 2020
Published online: October 1, 2020

[1] M. A. Green, A. Ho-Baillie, H. J. Snaith, *Nat. Photonics* **2014**, *8*, 506.
[2] M. Liu, M. B. Johnston, H. J. Snaith, *Nature* **2013**, *501*, 395.
[3] G. Grancini, C. Roldan-Carmona, I. Zimmermann, E. Mosconi, X. Lee, D. Martineau, S. Narbey, F. Oswald, F. De Angelis, M. Graetzel, *Nat. Commun.* **2017**, *8*, 15684.
[4] S. S. Shin, E. J. Yeom, W. S. Yang, S. Hur, M. G. Kim, J. Im, J. Seo, J. H. Noh, S. I. Seok, *Science* **2017**, *356*, 167.
[5] P. V. Kamat, *ACS Energy Lett.* **2018**, *3*, 28.
[6] J. Lin, M. Lai, L. Dou, C. S. Kley, H. Chen, F. Peng, J. Sun, D. Lu, S. A. Hawks, C. Xie, F. Cui, A. P. Alivisatos, D. T. Limmer, P. Yang, *Nat. Mater.* **2018**, *17*, 261.
[7] H. Cho, S.-H. Jeong, M.-H. Park, Y.-H. Kim, C. Wolf, C.-L. Lee, J. H. Heo, A. Sadhanala, N. Myoung, S. Yoo, S. H. Im, R. H. Friend, T.-W. Lee, *Science* **2015**, *350*, 1222.

[8] H. Sun, Z. Yang, M. Wei, W. Sun, X. Li, S. Ye, Y. Zhao, H. Tan, E. L. Kynaston, T. B. Schon, H. Yan, Z.-H. Lu, G. A. Ozin, E. H. Sargent, D. S. Seferos, *Adv. Mater.* **2017**, *29*, 1701153.
[9] J. Li, L. Xu, T. Wang, J. Song, J. Chen, J. Xue, Y. Dong, B. Cai, Q. Shan, B. Han, H. Zeng, *Adv. Mater.* **2017**, *29*, 1603885.
[10] W. Du, S. Zhang, J. Shi, J. Chen, Z. Wu, Y. Mi, Z. Liu, Y. Li, X. Sui, R. Wang, X. Qiu, T. Wu, Y. Xiao, Q. Zhang, X. Liu, *ACS Photonics* **2018**, *5*, 2051.
[11] S. W. Eaton, M. Laia, N. A. Gibsona, A. B. Wonga, L. Doua, J. Mac, L.-W. Wang, S. R. Leone, P. Yang, *Proc. Natl. Acad. Sci. USA* **2016**, *113*, 1993.
[12] Y. Fu, H. Zhu, C. C. Stoumpos, Q. Ding, J. Wang, M. G. Kanatzidis, X. Zhu, S. Jin, *ACS Nano* **2016**, *10*, 7963.
[13] Q. A. Akkerman, G. Raino, M. V. Kovalenko, L. Manna, *Nat. Mater.* **2018**, *17*, 394.
[14] F. Krieg, S. T. Ochsenbein, S. Yakunin, S. ten Brinck, P. Aellen, A. Suess, B. Clerc, D. Guggisberg, O. Nazarenko, Y. Shynkarenko, S. Kumar, C.-J. Shih, I. Infante, M. V. Kovalenko, *ACS Energy Lett.* **2018**, *3*, 641.
[15] J. Pan, S. P. Sarmah, B. Murali, I. Dursun, W. Peng, M. R. Parida, J. Liu, L. Sinatra, N. Alyami, C. Zhao, E. Alarousu, T. K. Ng, B. S. Ooi, O. M. Bakr, O. F. Mohammed, *J. Phys. Chem. Lett.* **2015**, *6*, 5027.
[16] S. Huang, Z. Li, L. Kong, N. Zhu, A. Shan, L. Li, *J. Am. Chem. Soc.* **2016**, *138*, 5749.
[17] A. Loiudice, S. Saris, E. Oveisi, D. T. L. Alexander, R. Buonsanti, *Angew. Chem., Int. Ed.* **2017**, *56*, 10696.
[18] H. Hu, L. Wu, Y. Tan, Q. Zhong, M. Chen, Y. Qiu, D. Yang, B. Sun, Q. Zhang, Y. Yin, *J. Am. Chem. Soc.* **2018**, *140*, 406.
[19] L. Wu, H. Hu, Y. Xu, S. Jiang, M. Chen, Q. Zhong, D. Yang, Q. Liu, Y. Zhao, B. Sun, Q. Zhang, Y. Yin, *Nano Lett.* **2017**, *17*, 5799.
[20] X. Zhang, X. Bai, H. Wu, X. Zhang, C. Sun, Y. Zhang, W. Zhang, W. Zheng, W. W. Yu, A. L. Rogach, *Angew. Chem., Int. Ed.* **2018**, *57*, 3337.
[21] B. Turedi, K. Lee, I. Dursun, B. Alamer, Z. Wu, E. Alarousu, O. F. Mohammed, N. Cho, O. M. Bakr, *J. Phys. Chem. C* **2018**, *122*, 14128.
[22] K. Shoyama, W. Sato, Y. Guo, E. Nakamura, *J. Mater. Chem. A* **2017**, *5*, 23815.
[23] L. Hongbo, Q. Yang, X. Xing, Z. Jianfeng, H. Xinyu, J. Qiang, Z. Weihua, Z. Chunfeng, L. Zhenda, *J. Phys. Chem. C* **2018**, *122*, 12994.
[24] S. Aparna, G. Richa, M. Shailaja, *J. Phys. Chem. C* **2017**, *121*, 14872.
[25] A. P. Schlaus, M. S. Spencer, K. Miyata, F. Liu, X. Wang, I. Datta, M. Lipson, A. Pan, X.-Y. Zhu, *Nat. Commun.* **2019**, *10*, 265.
[26] J. Atanu, K. S. Kim, *ACS Energy Lett.* **2018**, *3*, 2120.
[27] T. J. S. Evans, A. Schlaus, Y. Fu, X. Zhong, T. L. Atallah, M. S. Spencer, L. E. Brus, S. Jin, X.-Y. Zhu, *Adv. Opt. Mater.* **2018**, *6*, 1700982.
[28] K. Park, J. W. Lee, J. D. Kim, N. S. Han, D. M. Jang, S. Jeong, J. Park, J. K. Song, *J. Phys. Chem. Lett.* **2016**, *7*, 3703.
[29] Y. Wang, X. Li, J. Song, L. Xiao, H. Zeng, H. Sun, *Adv. Mater.* **2015**, *27*, 7101.
[30] S. Yakunin, L. Protesescu, F. Krieg, M. I. Bodnarchuk, G. Nedelcu, M. Humer, G. D. Luca, M. Fiebig, W. Heiss, M. V. Kovalenko, *Nat. Commun.* **2015**, *6*, 8056.
[31] A. Swarnkar, R. Chulliyil, V. K. Ravi, M. Irfanullah, A. Chowdhury, A. Nag, *Angew. Chem. Int. Ed.* **2015**, *127*, 15644.
[32] Q. Zhang, R. Su, X. Liu, J. Xing, T. C. Sum, Q. Xiong, *Adv. Funct. Mater.* **2016**, *26*, 6238.
[33] N. Yantara, S. Bhaumik, F. Yan, D. Sabba, H. A. Dewi, N. Mathews, P. P. Boix, H. V. Demir, S. Mhaisalkar, *J. Phys. Chem. Lett.* **2015**, *6*, 4360.
[34] G. Rainò, M. A. Becker, M. Bodnarchuk, R. F. Mahrt, M. V. Kovalenko, T. Stöferle, *Nature* **2018**, *563*, 671.
[35] L. Protesescu, S. Yakunin, M. I. Bodnarchuk, F. Krieg, R. Caputo, C. H. Hendon, R. X. Yang, A. Walsh, M. V. Kovalenko, *Nano Lett.* **2015**, *15*, 3692.
[36] X. He, Y. Qiu, S. Yang, *Adv. Mater.* **2017**, *29*, 1700775.
[37] Y. Gao, L. Zhao, Q. Shang, Y. Zhong, Z. Liu, J. Chen, Z. Zhang, J. Shi, W. Du, Y. F. Zhang, S. Chen, P. Gao, X. Liu, X. Wang, Q. Zhang, *Adv. Mater.* **2018**, *30*, 1801805.
[38] W. E. Samuel, L. L. Min, A. G. Natalie, B. W. Andrew, L. D. Tian, M. Jie, W. Lin-Wang, R. L. Stephen, P. D. Yang, *Proc. Natl. Acad. Sci. USA* **2016**, *113*, 13863.
[39] Q. Chen, J. Wu, X. Ou, B. Huang, J. Almutlaq, A. A. Zhumekenov, X. Guan, S. Han, Z. Yi, J. Li, X. Xie, Y. Wang, Y. Li, D. Fan, D. B. L. Teh, A. H. All, O. Mohammed, O. Bakr, X. Liu, *Nature* **2018**, *561*, 88.
[40] E.-P. Yao, B. J. Bohn, Y. Tong, H. Huang, L. Polavarapu, J. Feldmann, *Adv. Opt. Mater.* **2019**, *7*, 1801776.
[41] G. R. Yettapu, D. Talukdar, S. Sarkar, A. Swarnkar, A. Nag, P. Ghosh, P. Mandal, *Nano Lett.* **2016**, *16*, 4838.